Journal of Science and Technology

ISSN: 2456-5660 Volume 8, Issue 10 (Oct-2023)

www.jst.org.in *DOI:https://doi.org/10.46243/jst.2023.v8.i10.pp40- 57*

SPECTROSCOPIC MARK AND QUANTUM CHEMICAL INVESTIGATION FOR PHOTONIC/BIOLOGICAL APPLICATIONS

Mr S S Saravanakumar[a]

Guest Lecturer,

PG Research Department of Physics,

Sethupathy Government Arts College,

Ramanathapuram-623502, Tamilnadu India.

sgacsssphysics@gmail.com

Dr. M S Sameem[a*]

Assistant Professor,

Department of Chemistry,

M.S.S. Wakf Board College,

K K Nagar, Madurai District, Tamilnadu, India.

samnafil@gmail.com

Dr. P. Sivakumar[b]

Assistant Professor,

Department of Zoology

Arumugam Pillai Seethai Ammal College,

Sivagangai District, Tamil Nadu, India.

drsivaapsac@gmail.com

Dr. N. Sasirekha[c]

Guest Lecturer

Department of Zoology

Government Arts College for Women

Sivagangai district,

Tamilnadu in India.

smartsasi12@gmail.com

[a, a*] Corresponding Author, [b,c] Co authors

Journal of Science and Technology

ISSN: 2456-5660 Volume 8, Issue 10 (Oct-2023)

www.jst.org.in *DOI:https://doi.org/10.46243/jst.2023.v8.i10.pp40- 57*

To Cite this Article

Mr S S SaravanaKumar |Dr. M S Sameem |Dr.P. Sivakumar | Dr. N. Sasirekha,

"SPECTROSCOPIC MARK AND QUANTUM CHEMICAL INVESTIGATION FOR PHOTONIC/BIOLOGICAL APPLICATIONS" *Journal of Science and Technology, Vol. 08, Issue 10, OCT 2023, pp40-55*

Article Info

Received: 26-09-2023 Revised: 07-09-2023 Accepted: 17-10-2023 Published: 26-10-2023

Abstract

LGHCl - Semi-organic single crystals of L-Glutamic acid hydrochloride, optical material have been grown by the solvent evaporation route. Powder X-ray diffraction and FT-IR analysis confirmed the formation of LGHCl crystals. The optical second harmonic generation (SHG) conversion efficiency of LGHCl was determined by the Kurtz-Perry powder technique, and it is found to be 1.62 times that of potassium dihydrogen phosphate. Through the SHG dependency of average particle sizes, the relative SHG efficiency of the crystal and the phase matching characteristic of the crystal were explored. The dielectric behaviour of LGHCl single crystal as a function of temperature was examined (300–350 K). The crystal's photoconductive properties were investigated in order to determine its photocurrent and dark current responses. The Vickers microharness analysis at room temperature was used to evaluate the mechanical hardness of the generated LGHCl single crystal. Natural bond orbital (NBO) analysis was used to investigate the molecule's stability as a result of hyperconjugation and charge delocalization interaction. Furthermore, the total and partial density of states in the title compound was also determined. The obtained results indicate that the molecule is thermodynamically and optically stable, with a hyperpolarizability that is comparable to other molecules in its class.

Keywords: Crystal growth, LGHCl, PXRD, SHG, Natural bond orbital (NBO) analysis, Photoconductivity property, Photonic/Biological applications

Introduction

Optoelectronics, telecommunications, and the laser industry have all greatly benefitted from the use of second- and third-order nonlinear optical materials [1-3]. It has become essential for technological advancements in recent years to find NLO materials with substantial second and third-order optical nonlinearities and quick reaction times. Because of their high damage threshold, wide transparency range, lower UV cutoff wavelength, high nonlinear coefficient, high mechanical stability, and high thermal stability, semi-organic materials combine the enhanced properties of organic and inorganic crystals. This makes them ideal for frequency doubling and device fabrication. Organic ligands in semi-organic materials have hydrogen bonds with the inorganic network, leading to new high-optical nonlinear materials. Amino acids include zwitterions, which are carboxyl proton donor (COO-) and acceptor (NH_2) groups. Due to their dipolar nature, NLO applications can take use of their unique physical and chemical features [4]. Second harmonic generation (SHG) is one of the most exciting phenomena observed in most crystals without a symmetry centre and is used for frequency conversion, optical modulation, etc. Due to their high SHG efficiency and laser damage threshold (LDT) values, LiB_3O_5 (LBO), Lithium niobate ($LiNbO_3$), BaB (BBO), and others are employed for NLO applications [5-7]. However, creating defect-free crystals from the above components is arduous. Thus, photonic applications require a material with excellent NLO properties and easy single crystal formation. All amino acids except glycine have chiral carbon atoms and noncentrosymmetric crystal structures, making them good candidates for second harmonic and coherent blue-green laser generation [8, 9]. These crystals have SHG efficiency comparable to the aforementioned materials and can be formed utilizing slow evaporation solution growth (SESG) without melt growth methods. Molecular engineering and chemical synthesis allow amino acids to be modified and optimized [10].

In this present work, slow evaporation solution growth method was used to harvest a single crystal of L-Glutamic acid hydrochloride (LGHCl). For the synthesized material, PXRD, FTIR studies were carried out to identify the compound formation. Dielectric and Photoconductivity and micro hardness studies were also carried out for the grown crystals of the compound.

Furthermore, SHG phase matching studies for the LGHCl was carried out for the first time. First and second harmonic generation (SHG) theoretical approach and experimental methods were used to characterize the LGHCl crystal. Hyper conjugative interactions, charge delocalization, density of states and NBO analyses were used to determine the stability of the compound.

Experimental Analyses

Synthesis and crystal growth of LGHCl crystal

L-Glutamic acid was dissolved in deionized water and grew in an equimolar ratio with hydrochloric acid to form a single crystal of LGHCl. On the basis of the solubility data [11], it was decided to create a supersaturation solution and stir it for two hours. After being filtered and allowed to evaporate at room temperature, the solution was discarded. Using the slow evaporation solution growth method, optically transparent single crystals were grown in 25 days due to spontaneous nucleation. The technique of recrystallization improved the quality and size of the crystal. High quality, Colourless and optically transparent single crystals of LGHCl are harvested (Figure 1). Figure 2 depicts the Bravais-Friedal-Harker (BFDH) morphology of the crystal of LGHCl crystal.

Characterization procedures

PXRD investigation was performed on the generated LGHCl crystal using a Bruker AXS Advance X-ray diffractometer. The reference crystal was CuKα (=1.5406 Å), and the data was recorded.

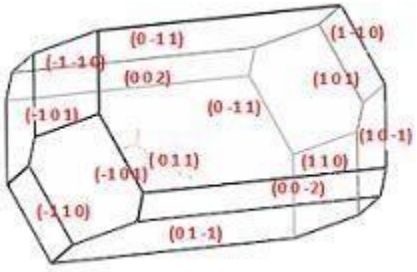

Figure 1 BFDH morphology of LGHCl

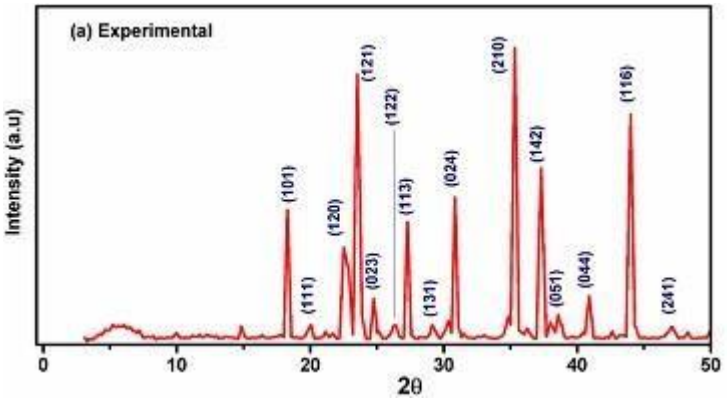

Figure 2 Powder XRD pattern of LGHCl

The FT-IR spectrum of the material was obtained using a Perkin Elmer spectrometer using the KBr Pellet technique in the range of 4000-400 cm^{-1}. The powder samples were carefully crushed to a particle size of 125-150 μm, and then they were loaded in a capillary tube with a diameter of around 1.5 mm. The power metre was used to determine the amount of input energy, and it came out to be 6 mJ/pulse. The laser employed used to have 1064 nm wavelength, a 8 ns pulse with, as well as 10 Hz repetition rate, and it was focused on the sample. The sample causes a green light emission at 532 nm, which is picked up with the aid of photomultiplier tube. The signal is first received by a photomultiplier tube, which transforms it into an electrical signal.

Using a Hioki 3532-50 LCR metre, a dielectric investigation was conducted in the frequency range of 50 Hz to 5 MHz at temperatures between 300 and 380 K. Utilizing Keithley-6517 B electrometer, the photoconductivity of an LGHCl crystal was measured. Under 100 mW/cm^2 of radiation, the photocurrent (IP) was measured for an applied voltage range of 1–10 V. Using an LEITZ WETZLAR apparatus equipped with a Vicker's hardness pyramidal indenter and an incident light microscope, the crystals' hardness was measured. For the determination of the hardness of LGHCl, single crystals of typical dimensions of 8x8x6mm3 ($l \times b \times h$) were used. The measured sample's volume and surface area are 0.73 cm^3 and 5.823 cm^2, respectively. Variable loads of 10g to 100g were used to create indentations on the surface of the grown crystal, which was placed correctly on the microscope's base. Five impressions were made for each weight, and

the optical microscope was used to determine the average pattern of diagonal lengths of the imprints.

Theoretical analysis details

All quantum chemistry calculations were performed using the Gaussian 09W software package [12] and the Becke-3-Lee-Yang-Parr (B3LYP) algorithm [12,13], with the standard 6-311++G(d,p) basis set for a single molecule. NBO 3.1 [14], a programme found in the Gaussian 09W software package, was used to do the NBO calculation. Utilizing NBO analysis, one can look at the potential for hyper conjugation and delocalization of various second-order interactions between full orbitals of one subsystem and unoccupied orbitals of another subsystem within the molecule [15]. The purpose of this study is to ascertain if interactions of this nature are actually realizable. Gauss View 5.0 is used to construct HOMO and LUMO orbitals for molecules at the frontier using the DFT/B3LYP/6-311++G(d,p) level of theory. Scientists have analyzed the HOMO-LUMO configuration to learn more about the molecule's electrical and optical properties, as well as its kinetic stability and chemical reactivity [15]. Important quantum chemical molecular properties, such as ionisation potential (IP), electron affinity (EA), electronegativity (v), electrophilicity index (x), chemical hardness (g), chemical softness (S), chemical potential (l), total energy change (DET), and overall energy balance (DE), have been calculated using the highest occupied molecular orbital (HOMO) and the lowest unoccupied molecular orbital (LUMO) [12-16].

Using the finite field approach theory, the first order hyperpolarizability (β) was determined. The magnitude of the first order hyperpolarizability tensor can be computed using the x, y, and z components.

First order hyperpolarizability is a third-rank tensor defined by a 3 x 3 x 3 matrix with 27 components; however, due to Kleinman symmetry [15], the number of components is decreased to 10. The output of Gaussian 09 lists the ten components of this matrix as *βxxx, βyxx, βxyy, βyyy, βzxx, βxyz, βzyy, βxzz, βyzz* and *βzzz* respectively. The components of the initial hyperpolarizability can be determined utilizing the following equations:

(1 a.u. = 8.6393 x 10- 33e.s.u.)

$\beta total$=(βx 2 + βy 2 + βz 2) ½ … (1)

where,βx = βxxx + βxyy + βxzz

βy = βyyy + βyzz + βyxx

βz = βzzz + βzxx + βzyy

Crystal classes determine the number of independent components of the second order hyperpolarizability tensor of the fourth rank. There are 81 independent non-zero elements in an orthorhombic system that are reduced by Kleinmansymmetry.

Using the equation [16], the second order hyperpolarizability value is computed.

γ = 1 5 ($\gamma xxxx$ + $\gamma yyyy$ + $\gamma zzzz$ + 2$\gamma xxyy$ + 2$\gamma xxzz$ + 2$\gamma yyzz$) … (2)

On the finite field method, the mean polarizability, the anisotropy of the polarizability, and the total static dipole moment can be defined using the following relations:

α = 1 3 (αxx + αyy + αzz) … (3)

$\Delta\alpha$ = 1 √2 [(αxx − αyy)^2 + (αyy − αzz)^2 + (αzz − αxx)^2 + 6αxy ^{2} + 6αyz ^{2} + 6αxz ^{2} … (4)

μ_{total}=(μx ^{2} + μy ^{2} + μz ^{2}) ½ … (5)

Result and Discussion

Powder X-ray diffraction analysis

The single crystal, fine powder of LGHCl was scanned in the 2θ range of 3° to 80°. Figure 2 depicts the powder XRD pattern that was recorded. The emergence of quite sharp and strong diffraction peaks demonstrated that LGHCl was crystalline and free from structural grain boundaries [14-16]. LGHCl crystal XRD [16] indicates that it is an orthorhombic system with the P212121 space group. The dimensions of the cell are a=5.1016(1) A°, b=11.6386(4) A°, and c=13.2500(3) A°. The actual and computed powder XRD patterns (2θ) agreed well with the JCPDS data (PDF no. 25-1925).

Optimized geometry

The experimental data and computed optimized structural parameters of LGHCl were both taken from the Gaussian'09 programme package using the B3LYP/6-311++G(d,p) level of theory and

X-ray diffraction data [16]. The results of comparing these two sets of information are shown in table 1. From table 1, it is evident that the differences between the experimental XRD data [15, 16] and the calculated geometric parameters are most likely caused by the interactions between molecules in the crystalline state. The difference could be explained by the fact that the calculations were done on a single molecule in the gaseous phase. In contrast to what was found in experiments, when many molecules are packed together, this is called the condensed phase.

Table 1 Optimized geometric parameters of L-Glutamic acid hydrochloride at B3LYP/6-311++G(d,p) level of theory

Bond lengths	B3LYP (Å)	XRD (Å)	Bond Angles	Dihedral Angles
Cl1-H9	1.8162	2.285	H3-O2-C12	H3-O2-C12-O4
O2-H3	0.9473	0.840	H7-O6-C21	H3-O2-C12-C13
N8-H9	1.0848	0.910	H11-N8-C13	H9-N8-C13-C12
C12-C13	1.5179	1.515	O4-C12-C13	H10-N8-C13-H14

Most of the optimized bond lengths are close to the experimental values. This is because molecules interact with each other. The N-H bonds with lengths of 1.084 Å, 1.0038 Å, and 1.006 Å, respectively. The NH...Cl and N-H...O intramolecular hydrogen bonds are what make the N8-H9 and N8-H11 bonds longer. The distance between Cl-H and O-H was found to be 1.821 and 2.191, which is much smaller than van darwaal's radii of 2.95 and 2.72. This suggests that N8-H9...Cl1 and N8-H11...O4 could form intramolecular hydrogen bonds. Due to the presence of electronegative Cl and O atoms, the hydrogen atoms next to each other in the NH^{3+} group, such as H9 and H11 and H10 and H11, move closer to each other. This makes the angles of the H-N-H bonds smaller than the angles of the H9-N8-H10 bonds.

Vibrational spectral analysis

The experimental FT-IR spectrum of the title compound is shown in Figure 3. The asymmetric stretching vibrations of NH_2 and the symmetric stretching vibrations of NH^2 are typically detected in the area 3380-3350 cm^{-1} and 3310-3280 cm^{-1}, respectively [16]. In amino acid

derivatives, the protonation of the NH^{3+} group 213 can cause a band position shift toward the region of 3300-3100 cm^{-1} and 3100-2600 cm^{-1}, respectively, for asymmetric and symmetric NH^{3+} stretching [13-16]. In the infrared spectrum, the stretching vibration bands caused by NH^{3+} appear to be wider and less intense than those caused by unmodified NH_2 groups. In the infrared spectrum, the asymmetric stretching mode of the NH^{3+} group can be seen at a frequency of 3147 cm^{-1} as a faint and broadband signal. In addition, the position, broadness, and wave number of the NH^{3+} asymmetric stretching mode of vibration point to the formation of a powerful N-H...Cl intra-molecular hydrogen bonding between the NH^{3+} group and the Cl- ion. This is indicated by the fact that the mode of vibration has a lower wavenumber. The existence of strong intermolecular and intramolecular N-H...Cl hydrogen bonding may be easily explained by the presence of the hydrogen bonding geometry of the LGHCl, which was also validated by the NBO analysis. This result suggests that there is robust hydrogen bonding between both ionic species, which produces the non-centrosymmetric structure and, as a result, contributes to the molecular hyperpolarizability in the LGHCl crystal. In the infrared spectrum, the asymmetric bending mode of the NH^{3+} ion may be seen as a faint band at 1674 cm^{-1}. The relatively powerful infrared band that was detected at 1509 cm^{-1} and assigned to the symmetric bending mode of vibration for NH^{3+}. The wavenumber range of 1295-1090 cm^{-1} is where the rocking vibrational modes of NH^{3+} can be found.

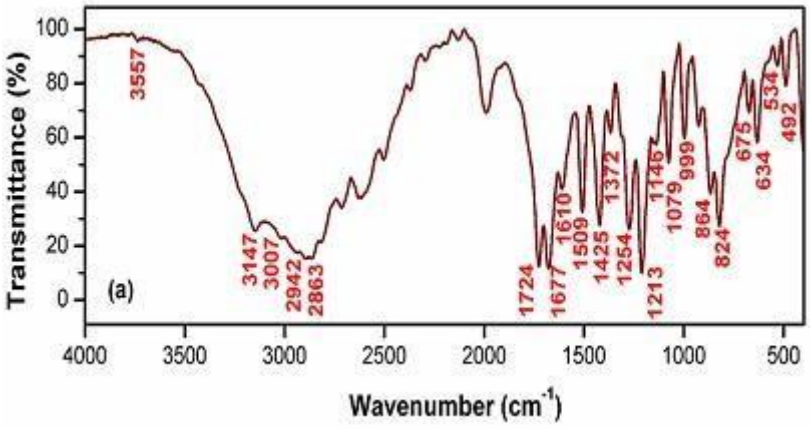

Figure 3 FTIR spectrum of LGHCl

Second Harmonic generation

The SHG efficiency ofLGHClis measured using Kurtz and Perry powder technique. The SHG efficiency was measured and compared with standard KDP. The SHG signals of 44 mV and 27 mV were obtained for LGHCl and KDP, respectively.

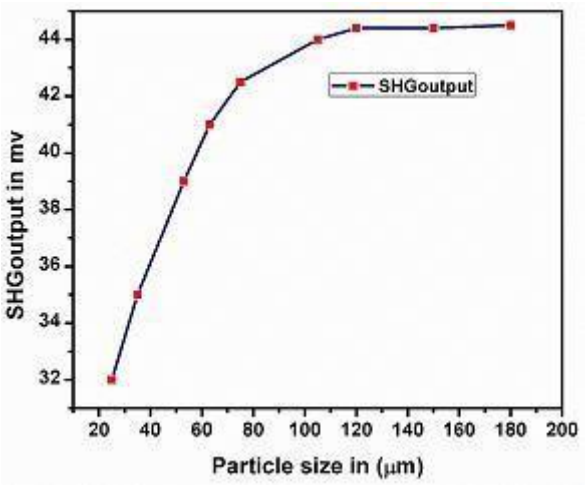

Figure 4 SHG output (mv) Vs Particle Size (μm)

From the figure 4, it can be concluded that the relative SHG efficiency of LGHCl is 0.67 times greater than that of standard reference KDP crystal.

Dielectric studies

Dielectric properties are fundamental electrical characteristics that are directly consistent with the electro-optic properties of crystals. The materials' dielectric properties are fundamental electrical properties. They offer vital detailsabout thepolarization process,defect activities and crystal structural activities. Low dielectric constant materials are needed in the microelectronics sector for interlayer dielectric The microelectronics industry is in need of low dielectric constant materials for use as interlayer dielectrics (ILDs), which can reduce RC delay, lesser power consumption, and decrease crosstalk between nearby interconnects [17, 18]. These benefits can be achieved by utilizing materials with a low dielectric constant. During the cooling process, dielectric tests were carried out on a specimen of the LGHCl crystal. It was possible to get the dielectric constant of the crystal by applying the following formula:

$\varepsilon r = Cd / \varepsilon_0 A$

where 'C' stands for capacitance, d for the crystal's thickness, 'A' for the crystal's cross sectional area, and 'r' for the free space permittivity (8.854 x 10-12Fm^{-1}). The dielectric constant as a function of frequency, and the dielectric loss are shown in figures 7a and 7b, respectively. At lower frequencies, both the dielectric constant (ε_r) and the dielectric loss (ε") increase, whereas at higher frequencies, they both decrease and reach a stable value. This occurs regardless of temperature.

The larger value of εr at lower frequencies may be due to the presence of space charge, orientation, electronic and ionic polarizations; the minimum value at higher frequencies is due to the progressive loss of consequence of the polarizations due to dipoles being unable to follow the applied electric field [19, 20]. The presence of space charge, orientation, electronic and ionic polarizations may also contribute to the larger value of εr at lower frequencies.

The change in dielectric constant that occurs with increasing temperature can be attributed to charge carriers and impurity dipoles that are thermally induced [21]. It was observed that the low dielectric constant (εr) of the LGHCl crystal is 16.5 at 343 K. This suggests that the LGHCl crystal may be a promising option for applications in electro-optic, photonic, and microelectronic device applications, particularly those that demand a rapid reaction.

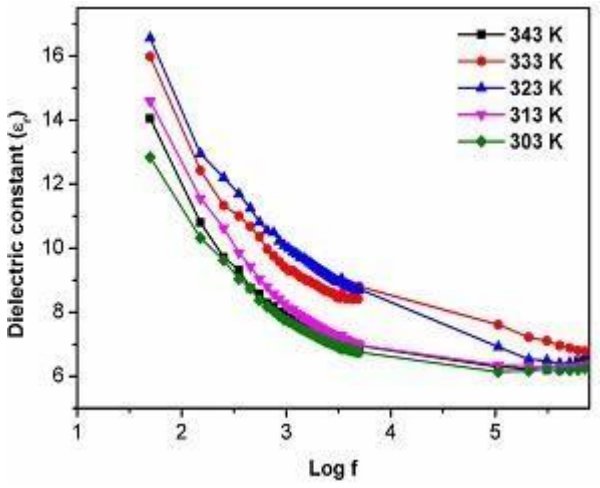

Figure 5 Dielectric Constant Vs Frequency

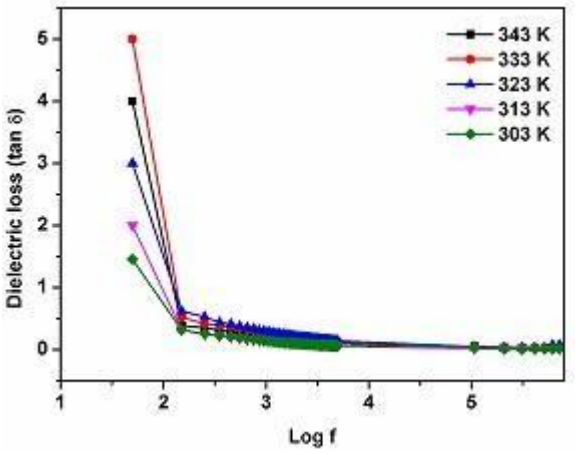

Figure 6 Dielectric loss Vs Frequency

For the purpose of increasing the SHG coefficient, appropriate parameters include the Miller rule as well as lower dielectric constant values at higher frequencies [20]. When the frequency is increased, the dielectric loss decreases. It is evidence that the LGHCl crystal is of high grade and contains fewer imperfections.

Photoconductivity study

The variation of field dependent dark current (Id) and photocurrent (Ip) measurements of the LGHCl crystal was carried out by a two probe technique at room temperature. The sample was shielded from radiation and the applied voltage rose from 1 V to 10 V in 1 V steps for dark current measurements.

A 100 W halogen lamp with iodine vapor and tungsten filament illuminated photocurrent measurements. Field dependence of dark current and photocurrent of LGHCl crystals is depicted in Figure 6. Clearly, the dark and photocurrent levels both grow linearly with the voltage level, but the photocurrent is comparatively smaller than the dark current value, which is known as negative photoconductivity. A two stage approach is supposed to explain negative photoconductivity in accordance with the Stockmann model. The energy level with the larger value can be found in the region between the conduction band and Fermi level. The energy level with the lower value can be found in the region near to the valence band. The lower energy level

features a capture cross section for electrons from the conduction band and holes from the valance band.

Presence of radiation, electron-hole recombination takes place and reduction of the number of mobile charge carriers exhibit the negative photoconductivity. [22] At ambient temperature, a fluctuation in the field dependent dark current (Id) and photocurrent (Ip) measurements of the LGHCl crystal was measured using a two-probe approach. In order to measure the dark current, the sample was shielded from any type of radiation sources, and also the supplied voltagewas incrementally increased insteps from 1 - 10 V range. For the purposes of photocurrent measurements, illumination was provided using a 100 W halogen lamp with a tungsten filament and iodine vapour contained within the bulb. The relationship between the field, dark and photocurrent values of LGHCl crystals is depicted in Figure 6.

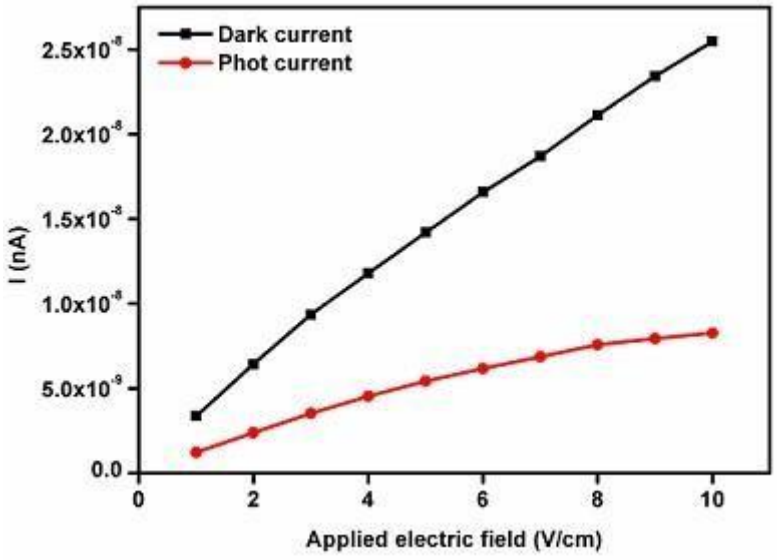

Figure 7 Photocurrent and dark current response of LGHCL with applied electric field

The term "negative photoconductivity" refers to the phenomenon in which the photocurrent is smaller than the dark current. It is obvious from the figure that both the dark and the photocurrent grows linearly with the increase in applied input voltage. The negative photoconductivity can be explained using a two-level approach, as suggested by the Stockmann

model. The energy level with the larger value can be found in the region between the Fermi level and the conduction band.

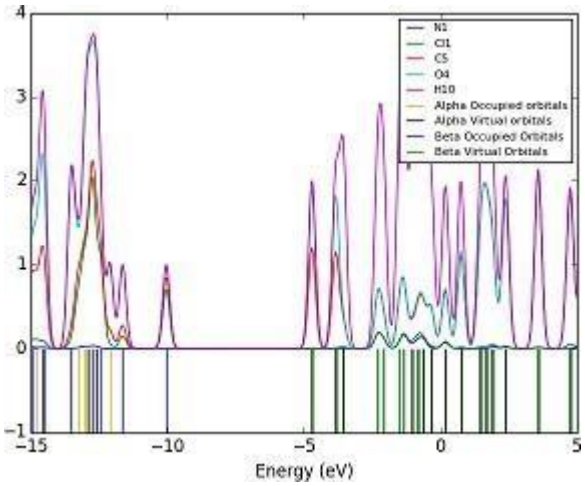

Figure 8 PDOS plot of LGHCl

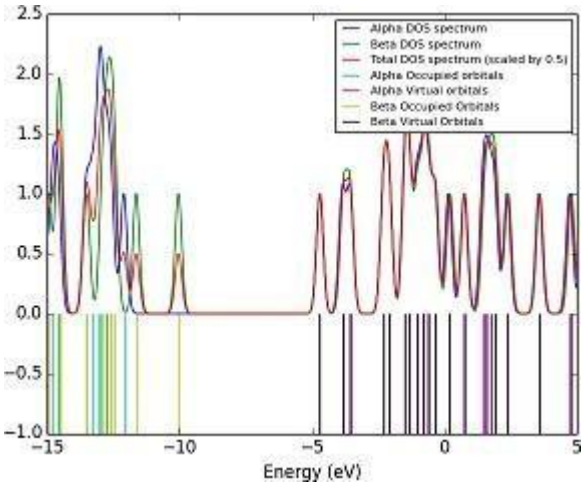

Figure 8 TDOS plot of LGHCl

The energy level with the lower value can be found in the region near to the valence band. The lower energy level features a capture cross section for electrons from the conduction band and holes from the valance band. In the presence of radiation, electron-hole recombination takes occur, which results in a decrease in the total number of mobile charge carriers, which demonstrates the negative photoconductivity effect [22].

Table 2 Calculated quantum chemical molecular orbital properties for LGHCl at DFT/B3LYP/cc-pVTZ method

Parameters	B3LYP/C6- 311++G(d,p)
HOMO energy, EHOMO (eV)	-7.3371
LUMO energy, ELUMO (eV)	-0.7434
HOMO- LUMO energy gap, ΔEGAP (eV)	6.5936
Ionisation potential, IP (eV)	7.3371
Chemical potential, μ (eV)	-4.0403

Conclusion

Using the slow solvent evaporation method, a semi-organic LGHCl single crystal has been produced. Powder X-ray diffraction (P-XRD) analysis validated the crystalline property of generated crystal. FT-IR spectroscopic technique have been used to examine the molecular vibrations of crystals of LGHCl. Using UV–vis absorption measurements, the range of optical transmission was determined; a peak was seen at 192 nm as the UV cutoff wavelength, and the band gap energy was also computed. The Second Harmonic Generation conversion efficiency of LGHCl is 1.62 times that of KDP crystal, the industry standard and the compound exhibits its phase matching behavior.

The values of the HOMO and LUMO energy gaps reflect the likelihood of charge transfer within the molecule. The first and second orderhyper polarizability are estimated at the B3LYP/6-311++G(d,p) level of theory. Thus, the aforementioned tests demonstrated that LGHCL could be a promising material for Second and third harmonic generation NLO applications as well as biological applications.

REFERENCES

[1] Acharya, K. P.: Photo current Spectroscopy of CdS/ Plastic, CdS/Glass, and ZnTe /Ga As Hetero-pairs Formed with Pulsed Laser Deposition. Ph.D. Thesis, Bowling Green State University, 2009.

[2] Bhattacharya, R.; Saha,S.: Growth of CdS Nanoparticles by Chemical Method and its Characterization. Pramana-Journal of Physics 2008, 71, 187-192.

[3] S.A. Empedocles, R. Neuhauser, K. Shimizu and M.G. Bawendi, Adv. Mater., 11 (1999) 1243–1256.

[4] M. Sabet, M. Salavati-Niasari and O. Amiri, Electrochim. Acta, 117 (2014) 504–520.

[5] O. Amiri, M. Salavati-Niasari, A. Rafiei and M. Farangi, RSC Adv., 4 (2014), 62356–62361.

[6] O. Amiri, M. Salavati-Niasari, S. M. Hosseinpour-Mashkani, A. Rafiei and S. Bagheri, Mater. Sci. Semiconduct. Process., 27 (2014), 261–266.

[7] X. Duan, Y. Huang, R. Agarwal and C.M. Lieber, Nature, 421 (2003) 241–245.

[8] M.V. Artemyev, V. Sperling and U. Woggon, J. Appl. Phys., 81 (1997) 6975–6977.

[9] A. Hagfeldt and M. Gratzel, Chem. Rev., 95 (1995) 49–68.

[10] V.L. Colvin, M.C. Schlamp and A.P. Alivisatos, Nature, 370 (1994) 354–357.

[11] X.G. Peng, M.C. Schlamp, A.V. Kadavanich and A.P. Alivisatos, J. Am. Chem. Soc., 119 (1997) 7019–7029.

[12] X. Liu, Mater. Chem. Phys., 91 (2005) 212–216.

[13] D. Ghanbari, M. Salavati-Niasari, S. Karimzadeh and S. Gholamrezaei, J. NanoStruct., 4 (2014) 227–232.

[14] G. Nabiyouni, S. Sharifi, D. Ghanbari and M. Salavati-Niasari, J. NanoStruct., 4 (2014) 317–323.

[15] M. Panahi-Kalamuei, M. Mousavi-Kamazani and M. Salavati- Niasari, J. NanoStruct., 4 (2014) 459–465.

[16] F. Beshkar and M. Salavati-Niasari, J. NanoStruct., 5 (2015) 17–23.

[17] V. Mathew, S. Jacob, C. K. Mahadevan and K. E. Abraham, Phys. B, 2012, 407, 222–226.

[18] P. Srinivasan, T. Kanagasekaran, N. Vijayan, G. Bhagavannarayana, R. Gopalakrishnan and P. Ramasamy, Opt. Mater., 30 (2007) 553–564.

[19] K. Syed, S. Babu, G. Peramaiyan, M. Nizam Mohideen and R. Mohan, J. Therm. Anal. Calorim., 120 (2015) 1337–1345.

[20] Broadband Dielectric Spectroscopy, ed. F. Kremer and A. Schoenhals, Springer, Berlin, 2003.

[21] S. Nazarath Begum, U. Sankar, T. ChithambraThanu and P. Selvarajan, Optik, 125 (2014) 1493–1497.

[22] M. Narayana Bhat, S.M. Dharmaprakash, J. Cryst. Growth 236 (2002) 376–380.

Statements & Declarations

We confirm that the manuscript has been read and approved by all named authors and that there are no other persons who satisfied the criteria for authorship but are not listed. We further confirm that the order of authors listed in the manuscript has been approved by all of us.

Data Availability Statement

The authors confirm that the data supporting the findings of this study are available within the article.